Niu, Xun; Huan, Siqi; Li, Haiming; Pan, Hui; Rojas, Orlando J.

Transparent films by ionic liquid welding of cellulose nanofibers and polylactide

Published in:
Journal of Hazardous Materials

DOI:
10.1016/j.jhazmat.2020.124073

Published: 15/01/2021

Document Version
Publisher's PDF, also known as Version of record

Journal of Hazardous Materials 402 (2021) 124073

Contents lists available at ScienceDirect

Journal of Hazardous Materials

journal homepage: www.elsevier.com/locate/jhazmat

Transparent films by ionic liquid welding of cellulose nanofibers and polylactide: Enhanced biodegradability in marine environments

Xun Niu [a,b], Siqi Huan [b], Haiming Li [c], Hui Pan [a,*], Orlando J. Rojas [b,d,**]

[a] College of Chemical Engineering, Nanjing Forestry University, 159# Longpan Road, Nanjing 210037, China
[b] Bioproducts Institute, Departments of Chemical and Biological Engineering, Chemistry and Wood Science, University of British Columbia, Vancouver, BC V6T 1Z3, Canada
[c] School of Light Industry and Chemical Engineering, Dalian Polytechnic University, Dalian, Liaoning 116034, China
[d] Department of Bioproducts and Biosystems, School of Chemical Engineering, Aalto University, Espoo FI-00076, Finland

ARTICLE INFO

Keywords:
Polylactide
Cellulose Nanofibers
Ionic liquid welding
Degradation
Seawater

ABSTRACT

We introduce a green and facile method to compatibilize hydrophobic polylactide (PLA) with hydrophilic cellulose nanofibers (CNF) by using ionic liquid ([DBNH][OAc]) welding with a cosolvent system (gamma-valerolactone). Such welding affords strong (230 MPa tensile strength), flexible (13% elongation at break), transparent (>90%) and defect-free CNF/PLA films. The films are biodegradable in marine environments (70% degradation in 7 weeks), facilitating the otherwise slow PLA decomposition. Physical, chemical and structural features of the films before and after welding are compared and factored in the trends observed for degradation in seawater. The results point to the possibility of PLA-based films forming a co-continuous system with nanocellulose to achieve an improved performance. The role of film morphology, hydrophobicity, and crystallinity is discussed to add to the prospects for packaging materials that simultaneously display accelerated degradability in marine environments.

1. Introduction

Nanoscale building blocks (plate-like, fibrillar, or spherical) (Raquez et al., 2013) have long been considered as desirable components in composite materials to tailor their structural (porosity, surface area, and networking) and physical (e.g., density, permeability, strength, and thermal stability) properties and to endow given functions and uses (e.g., catalysis, antimicrobial, biodegradability, thermal/electrical conductivity, among other) (Fernandes et al., 2013; Rhim et al., 2013). Two-dimensional structures comprising cellulose nanofibers (CNF) exploit the high axial aspect of the nanomaterial, its superior mechanical moduli, and biodegradability. CNF functions as nanoscale building block in nanocomposites, offering great potential in separation, packaging, catalysis, energy harvesting, sensing, and actuation (Zhu et al., 2016).

Bio-based polymers, such as polylactic acid (PLA), have been introduced to tackle the "white pollution" from fossil carbon. CNF-reinforced PLA has been of great interest in preparations that dominantly depends on the dispersion state of the CNF in the matrix. The latter has been tailored by melting (Clarkson et al., 2018; Sharif et al., 2019), thermo-kinetic mixing (Oguz et al., 2019; Wu et al., 2019), or solution casting (Le Phuong et al. 2019; Muiruri et al, 2019). Unfortunately, the results so far indicate inefficient mixing and compatibilization. To address these challenges, nanocellulose chemical modification (Rol et al., 2019) or coupling with additives, such as amphiphilic molecules, including proteins (Ahn et al., 2018; Khakalo et al., 2018), surfactants (Kaldéus et al., 2019), and fatty acids (Soman et al., 2017) have been attempted with some success. Unfortunately, these approaches demand tedious, multistep processes that come with a cost (materials, and environmental risks). Moreover, gains in composite elongation, a desirable property for processing, generally develops with a trade-off compared to other properties, such as tensile strength (Meng et al., 2018). Hence, there is still a need for cost-effective and facile methods to develop flexible and compatible CNF/PLA composites.

Natural fiber welding allows the manipulation of inexpensive and renewable materials with limited disruption of their native structures

* Corresponding author.
** Corresponding author at: Bioproducts Institute, Departments of Chemical and Biological Engineering, Chemistry and Wood Science, University of British Columbia, Vancouver, BC V6T 1Z3, Canada.
E-mail addresses: hpan@njfu.edu.cn (H. Pan), orlando.rojas@ubc.ca (O.J. Rojas).

https://doi.org/10.1016/j.jhazmat.2020.124073
Received 6 August 2020; Received in revised form 14 September 2020; Accepted 21 September 2020
Available online 22 September 2020

(Haverhals et al., 2010). For example, the outer regions of a fiber can be modified preferentially, while its core preserved in the native state (Durkin et al., 2016). Welding has been used to process silk (Brenckle et al., 2016), cotton (Haverhals et al, 2012a), cellulose microfibers (Yousefi et al., 2011), and CNF (Reyes et al., 2018). Typically, the welded materials have shown enhanced connectivity and high structural integrity, allowing good stress transfer through the continuous network of the reinforced matrix (Haverhals et al, 2012b). For this purpose, ionic liquids (ILs) have shown a reduced tendency to decompose the polymer matrix during processing; meanwhile, the presence of finely dispersed nanofillers promotes crystal formation in the composite (Gardella et al., 2015).

The degradation of PLA in soil has been addressed in a number of studies, some of which suggest that accelerated degradation can be achieved when PLA is combined with cellulose (Yang et al., 2015). The results point to the well-known fact that biodegradation occurs only under certain conditions depending on temperature, humidity, light, oxygen, and microorganisms availability, among others (Xu et al., 2019). Unfortunately, few studies available on the degradation of PLA in aquatic environments indicate a very slow degradation rate (~280 days) (Urbanek et al., 2018). To comprehensively scrutinize "biodegradable polymers", it is essential to understand the degradation tendency as well as products of degradation in "real" aquatic conditions. Likewise, the effect of additives needs to be considered in a life cycle assessment.

Herein, we report a method to enhance the physical-mechanical properties of CNF/PLA composite films by a simple and green welding process using an IL ([DBNH][OAc]) with gamma-valerolactone (GVL) co-solvent to lower the cost and processability under mild conditions. The developed nanocomposites featured a layered structure in which PLA and CNF form a co-continuous system, where the fibrils act as reinforcing agent, with no evidence of phase separation. The results indicate a synergistic effect, whereby the composites show high toughness and flexibility (24 MJ/m^3, 13%). Importantly, the welding treatment enhances the biodegradation in marine conditions. The role of film morphology, hydrophobicity, and crystallinity is discussed to add to the prospects for packaging materials.

2. Experimental section

2.1. Chemicals

Bleached Kraft softwood pulp (BKP) was provided by a Finnish pulp mill. The BKP was microfluidized (Microfluidics M-110P™, International Corporation, USA) into cellulose nanofibrils (CNF) with an average diameter of 37 nm (see TEM image in Fig. S1). Commercial poly (lactic acid) (PLA) latex was provided by Miyoshi Oil& Fat Co., Ltd. (Japan), with a solid content of 40 wt% and an average particle size of 1 μm. [DBNH][OAc] was kindly provided by Helsinki University. Gamma-valerolactone and acetone were purchased from Sigma Aldrich (USA). All chemicals were used as received.

2.2. Preparation of CNF/PLA films

CNF and PLA latex were each firstly diluted with Milli-Q water to 0.5 wt% concentration. For this, the respective suspension was vigorously stirred and sonicated in an ice bath in tightly closed bottles. The CNF and PLA suspensions were then mixed (magnetic stirring, one day) at a weight ratio of 50:50. The mixture was next filtrated with a polyvinylidene fluoride filter membrane (Durapore GVWP14250, 142 mm diameter, 0.22 μm pore size) at 2.5 bar for 1 h. The obtained gel-like cake was wet-pressed between two blotting papers followed by hot-pressing in a Carver Laboratory press (18200-213, Freds, Carcer Inc. USA) at 80 °C, 1500 Pa, covered between two metallic substrates. After 2 h, the films were dried and peeled off from the filter. The dried CNF/PLA samples were cut into squares (3 × 3 cm^2) and denoted as C/P. The obtained samples were stored at 23 °C, 50% RH until further use (see Fig. 1 for a schematic illustration of the procedure used). Note: A small amount of dispersing agent is expected in the PLA emulsion (data unknown). Unfortunately, no details about the type and content are provided, given that this is a commercial product. That is probably part of their patents not open to the public. It is possible that during the several procedures applied, using water and solvent, the surfactant is removed from the composition but this is difficult to confirm, given the extremely high dilution.

2.3. Fabrication of IL-welded films

A series of tensile tests were conducted to investigate the different factors affecting the mechanical properties of CNF/PLA films welded by different ILs and co-solvent systems. The experiments suggested that the mechanical properties of CNF/PLA composite films can be tailored by controlling the IL type, co-solvent, and welding time. Except for the IL type used in this work, all the other solvents gave sub-optimal results (adhesive films, difficult to handle, poor properties). The best results were obtained with the reported IL and, to lower its cost, only 5% was used in the composition (with 95% GVL as co-solvent). Such system can be recycled and reused (data not shown based on double-solvent extraction combined with an anti-solvent precipitation process for a

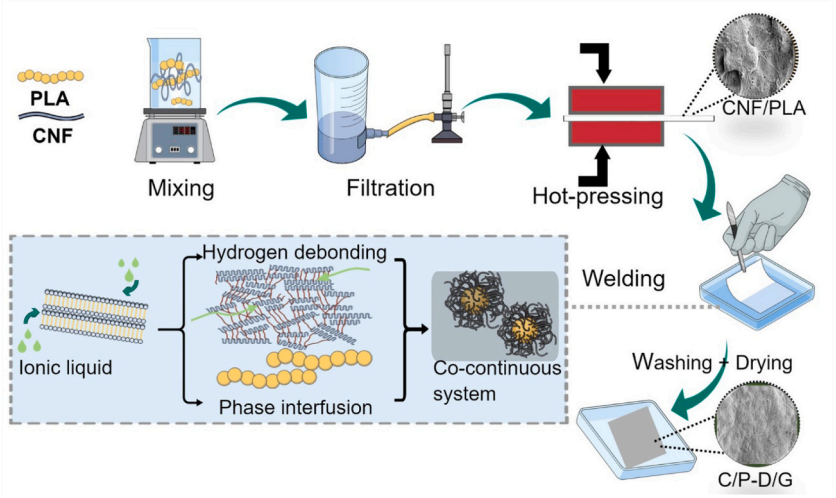

Fig. 1. Schematic illustration of the procedure used for the synthesis of CNF/PLA films via welding with IL [DBNH][OAc] and a co-solvent, GVL (the obtained films are referred to as "C/P-D/G").

maximum recovery rate of 98%). The IL choice was further based on a compromise between cost and superior properties, as shown in Fig. S2 for films produced from different IL systems. Notably, C/P treated with IL for 1 h exhibited the highest elasticity and based on the results, GVL was chosen as cosolvent with [DBNH][OAc] at a ratio of 95/5 (wt%). We investigated different CNF/PLA ratios, 90:10, 70:30, and 50:50. The latter composition was used since it produced the least phase separation and shrinkage. CNF/PLA films were immersed in the liquid IL system ([DBNH][OAc]/GVL) and turned over after 1 min (for a total time of 2 min to complete the process). Thereafter, the respective wet CNF/PLA film was allowed to weld by placing it on a glass Petri dish during given time (1 min, 1 h, and 5 h under ambient conditions). The impregnated samples were then washed with acetone to remove residual IL and transferred to distilled water. Then, the films were dried at 80 °C with a Carver Laboratory press (under a low loading, 1500 Pa). The [DBNH][OAc]/GVL welded CNF/PLA film is thereafter denoted as "C/P-D/G" (see Fig. 1). All prepared samples were stored at 23 °C, 50% RH until further use.

2.4. Characterization

The thickness (μm) of the films was measured using a micrometer at six random positions and the average value is reported. The porosity was calculated based on density determinations. Scanning electron microscopy (SEM, Zeiss Sigma VP) was used to image the surface and the cross-sectional morphologies of the films. Fractured film samples were obtained from the uniaxial tension for tensile properties, sputtered with a 3 nm platinum film (Emitech K100X) and imaged at 1 − 3 kV acceleration voltage. X-ray diffraction Ultima IV X-ray diffractometer (XRD, Rigaku, Smartlab, Japan) was used to investigate the crystalline patterns and crystal index of PLA and CNF. Transmittance spectra of the films were recorded in the UV−visible range with PerkinElmer Lambda 950 UV/vis/NIR absorption spectrophotometer. The water contact angle (WCA) was determined using a Theta Flex optical tensiometer from Biolin Scientific at a RH of 50% and 23 °C, each contact angle was taken at 60 s, and the average value of at least three measurements is presented. Water absorption of the films was determined by placing circular film (4 cm diameter) into Petri dishes with deionized water and calculated based on the change in weight before and after 30 min immersion. The tensile strength, Young's modulus, and elongation at break of the film samples were obtained with an Instron 4204 universal testing machine, with a gauge length at 10 mm, a 100 N loading cell, and a crosshead speed of 5 mm/min. Dynamical mechanical analyses (DMA) were carried out in creep/relaxation mode using the Q800 instrument (TA Instruments, USA). For this, the films were cut into strips with a width of 5.3 mm and tested by applying multiple 10 MPa stress/no-load cycles at different levels of relative humidity (10%, 30%, 50%, 70%, and 90% RH) and a constant temperature of 30 °C. Degradation tests were conducted by immersing the film samples (1.2×1.2 cm^2) in 3 ml marine water (collected in the bay, Gulf of Finland) in vials carrying caps with holes to facilitate oxygen exchange with the environment. All samples were stored for over a month in a chamber at constant temperature (25 °C) and under controlled fluorescent illumination (16-h on and 8-h off during per day). The medium was replaced every two weeks.

3. Results and discussion

3.1. Film morphology

Pursuing our interest in degradable CNF/PLA composite films with superior mechanical performance, we firstly tested a series of IL-welded C/P films considering factors involving (1) IL type ([N_{4444}][OAc]-TBAA, [DBNH][OAc]-DB, [mTBNH][OAc]-TB, and [EMIM][OAc]-EMIM); (2) co-solvent (GVL, and DMSO) and (3) welding time (1 min, 1 h, and 5 h). The welded C/P samples were prepared in light of the above factors and taken into consideration the stress-strain profiles (Fig. S2**).** A combination of [DBNH][OAc] and GVL yielded the best results; meanwhile, this IL system presented a low viscosity to enable easy washing and recycling. The film thicknesses, density and porosity of the composite films are summarized in Table S1. The thickness of C/P was 24 ± 0.3 μm. IL welding led to a reduction in thickness, from 22 ± 0.1 μm (C/P-D/G 1 min) to 19 μm (C/P-D/G 5 h), with a corresponding increase in density after 5 h welding, from 1.25 g/cm^3 to 1.32 g/cm^3. The porosity, determined as the ratio of the void space to the total volume of the film, decreased with welding time (13% and ~9%, before and after 1 h, respectively).

SEM analysis of the surface and cross-section of both C/P and C/P-D/G samples were performed. As shown in Fig. 2a, the non-welded C/P film (produced with CNF and PLA latex) presented phase separation. PLA latex (shown in circles in Fig. 2) and overlaid CNF aggregates were observed (plane view). Vertically aligned fibers and micro-sized particles can be seen in the cross-section (Fig. S3a). After 1 min welding treatment with [DBNH][OAc]/GVL, the original rough surface of C/P film became smoother (Fig. 2b) and aggregation size was reduced. Straight cracks were observed in cross-sections (Fig. S3b), indicating the IL welding effect. Notably, the C/P-D/G (1 h) sample showed a more continuous and relatively homogeneous surface (Fig. 2c), which is likely due to partial CNF dissolution under the longer welding time. As a result, the dissolved CNF filled the space between CNF bundles and PLA particles, in stacked layers, forming a better dispersion. A lamellar structure was produced but with an increased characteristic width. Further extending the welding time to 5 h resulted in a smoother surface, with a structure reminiscent of that observed for CNF nanopapers. A physically entangled CNF network was apparent in the high-magnification image (Fig. 2d). Moreover, compared to the un-welded C/P film, Fig. 2a, much less CNF aggregation was observed, suggesting a better dispersion of CNF upon welding. The results correlate with the cellulose-dissolving ability of IL, used here as an efficient agent for the dispersion of nanofibers from bundled structures. Welding influenced the individual nanofiber density, distribution, and diameter on the surface. These results confirm the change in porosity and density of the composite films.

3.2. Structural properties

XRD profiles of the C/P and C/P-D/G samples indicated the changes in crystallinity for different welding times (Fig. 3a). The two overlapped peaks at $2\theta = 14.0$–$17.8°$ and the diffraction peak at $2\theta = 22.5°$ correspond to the (101), $(10\bar{1})$, and (200) crystal planes of cellulose I crystalline structure, respectively (Min et al., 2020). The peaks at 19.1° and 16.5° correspond to the α crystallites and amorphous PLA (Li and Qiu, 2019). After IL welding, the diffraction peaks did not show any apparent shift, suggesting the absence of significant changes in the crystals. The intensity changes of cellulose planes confirmed partial dissolution of CNF during welding and the crystallinity index (CI) decreased from 70% (C/P) to 66% (C/P-D/G 1 min). After 1-h and 5-h welding CI values were 72% and 63%, respectively. The slight CI increase of C/P-D/G 1 h is likely due to an effect similar to that of defibrillation of wood fibers into CNF: 1 min is insufficient for dissolution of non-ordered cellulose, while an excessive time (5 h) produces extensive dissolution. An intermediate time, 1 h, gives a balance as far as exposing the crystalline cellulose. The total weight loss of C/P composite film upon welding supports the observations; the sample with the highest CI lost up to 11% of its initial weight due to dissolution in the IL. Further, as shown from deconvolution of the XRD patterns (Fig. S4), compared to C/P, the full width at half-maximum (FWHM), $2\theta = 16.5°$, of the composite films became smaller. The C/P-D/G samples showed a lower FWHM value than that of C/P; accordingly, following the Scherrer formula, there is an increased generation of bigger PLA crystals in the composite films (Patterson, 1939; Yu et al., 2017), which may further lead to a lower impact resistance. This result is supported by Park and Xanthos (2009) who found that shorter chains of PLA are more susceptible to crystallize due to

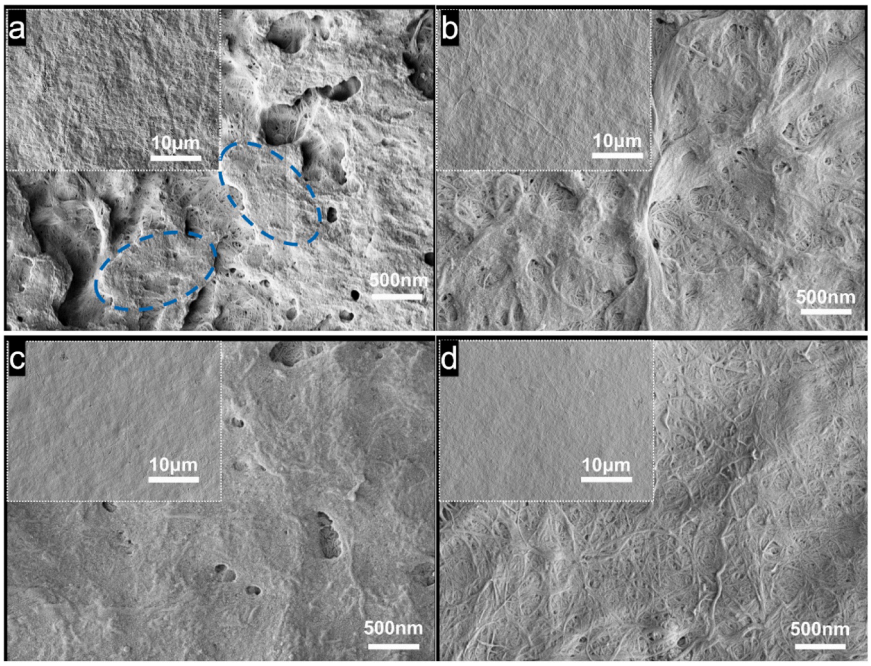

Fig. 2. SEM images of fractured film surfaces at 10,000× magnification (insets correspond to 1000× magnification): (a) C/P; (b) C/P-D/G 1 min; (c) C/P-D/G 1 h; (d) C/P-D/G 5 h.

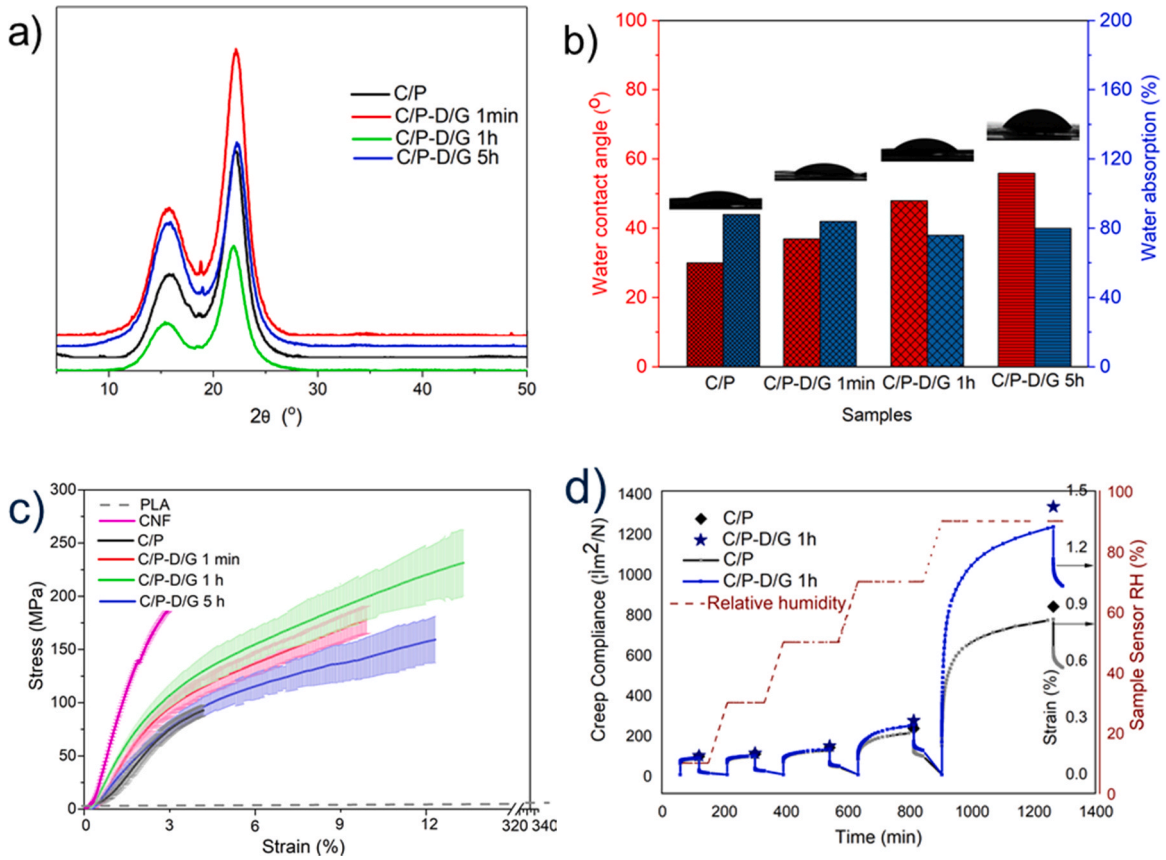

Fig. 3. (a) XRD patterns, (b) water contact angle and water absorption, and (c) stress-strain profiles (the standard deviation is shown as highlighted areas around the different profiles) for composite films (C/P, C/P-D/G 1 min, C/P-D/G 1 h, and C/P-D/G 5 h). (d) Creep compliance and strain in multiple creep-recovery cycles (the scattered lines refer to compliance and line +symbol refer to strain) at 10–90% RH (30 °C) of the films (C/P, C/P-D/G 1 h).

IL-induced mobility.

3.3. Optical properties

The light transmittance profiles of the nanocomposite films are shown in Fig. S5a, and indicate agreement with the conclusions derived from the SEM images of the fractured surfaces. The C/P-D/G films presented only a slightly lower transparency (about 2% lower) compared to the unwelded film. The light transmittance of the C/P-D/G films was higher than that of polyethylene (PE, <88.6%) (Lin et al., 2019), polyethylene terephthalate (PET, <90.2%) (Zhang et al., 2019), and the corresponding isotropic film (90.5%) (Wang et al., 2016), as well as the anisotropic cellulose films (87.3%) (Ye et al., 2019; Zhu et al., 2017).

IL welding increased the interconnection between CNF and the PLA latex and formed a layered but loose structure. The large and initially aggregated cellulose fibrils formed a randomly intertwined network partially filled by PLA latex, via a co-continuous and well-dispersed surface; as a result, the refractive index variation and scattering at the interfaces were minimized, which led to nanocomposites of high optical transparency (transmittance >90%). The 1-min IL welded CNF/PLA film exhibited a 10% haze increase compared to the neat C/P film (~15%, Fig. S5b). The haze of the resultant D/G-treated 1 h C/P was doubled than that of native C/P (~30%). The slight increase in haze is explained by the randomly intertwined CNF network and the IL-induced mobility of PLA latex during the fabrication of the composite enhancing light scattering.

3.4. Water interactions

The interactions with water were evaluated by measuring the water contact angle (CA). The composite films after IL welding had a higher CA than the C/P sample: it increased from 30° for the neat C/P to 48° for films after 1-h welding and 56° with 5-h welding (Fig. 3b**)**. Generally, PLA films have a CA in the range 70–80° (Gordobil et al., 2015; Jamshidian et al., 2012), while CNF films have a CA of 30–60° (Deng et al., 2017; Spence et al., 2010; Zhu et al., 2016). C/P had the roughest surface (SEM) that may cause CA variations while the semi-crystalline cellulose with its surface hydroxyls and structural heterogeneity (Rodionova et al., 2012) enhances the hydrophilicity.

Moisture absorption was evaluated by immersing the films into water until reaching equilibrium, over a time period of 600 s. A denser structure, with fewer pores makes it easy for water to be retained, by as much as ~55% for CNF/PLA films. After welding, water absorption was decreased by more than 30% over 60 min (Fig. 3b). The significantly decreased water absorption of IL-welded films is related to (1) changes in porosity, e.g., caused by the increased interconnection of CNF and PLA by IL, especially the void-filling effects of PLA (Table S1). (2) Surface hydrophobicity since the C/P-D/G welding for up to 5 h showed a higher water absorption after dissolution of CNF. The enhanced moisture sensitivity of the composite films indicated that the chemical interactions between PLA and CNF and the nanostructure containing well-dispersed PLA latex in a moisture-sensitive matrix made the films stable in humid environments.

Fig. 3c shows the stress–strain curves of CNF and C/P films as well as the corresponding welded films. The neat CNF film has a tensile strength of 188 MPa, a fracture strain of 2.9%, a toughness of 2.8 MJ/m^3, and a Young's modulus of 7.1 GPa. The results indicate a stiff and brittle material. In contrast, PLA is a soft and ductile material. Our results indicate that treatment for 1 min produced a fall in tensile strength, toughness, and Young's modulus (95 MPa, 1.8 MJ/m^3, and 3.2 GPa, respectively). In contrast, the fracture strain increased to 4%. Significantly, the best mechanical performance was achieved by the C/P-D/G composite film subjected to 1 h welding time: the corresponding tensile strength, fracture strain, toughness, and Young's modulus are 231.3 MPa, 12.9%, 23.8 MJ/m^3, and 5.4 GPa.

The experimental results show that a short IL treatment time effectively enhances the mechanical properties of the CNF/PLA composite film. First, the substantial increase in strength of C/P-D/G relates to the adhesion properties of the IL, as it has been reported to be strong and effective solvent for weakening cellulose interfibrillar hydrogen bonding as well as partial dissolution, forming a co-continuous system (dissolved cellulose and CNF) (Tripathi et al., 2018; Wang et al., 2012; Zhang et al., 2017). Upon observing the surface of the films (SEM in Fig. 2a), the dissolved cellulose is shown to connect the smaller-sized CNF with PLA particles. Thus, upon welding, dissolved cellulose, CNF, and PLA latex form a co-continuous system where CNF/PLA becomes better integrated while presenting more limited phase separation, leading to an increased area for stress transfer.

3.5. Creep/recovery cycles

Packaging materials in practical use suffer from moisture and mechanical stress during their lifetime and disposal. To investigate the synergistic effect of moisture and load, creep/recovery cycles of IL-welded CNF/PLA films under different humidity were examined (Figs. 3d and S6**)**. The results point to the fact that the deformation of composite films remained fairly unchanged until reaching a RH of 70%. Obviously, the deformation of the IL-welded sample was significantly higher than that of the C/P, and the difference became even more pronounced with increased RH. A sharp increase of creep and reduced ability to recover the original strain were observed at high humidity. For instance, the welding effect increased the creep compliance and strain (from 220 to 260 μm^2/N and from 17% to 26%) at 70% RH. Moreover, at 90% RH, the aforementioned properties further increased by ~60% (from 825 to 1322 μm^2/N and from 8% to 13%). It is generally accepted that cellulose can undergo water-induced plasticization and a high moisture content leads to accelerated degradation of cellulose products, on the basis of static physical tests (Olsson et al., 2007). Here, the more pronounced creep from IL-welded samples not only correlated with the presence of CNF but possibly, the better dispersion and stronger interactions between the PLA and CNF, resulting in a composite that is more resistant to failure. The state of dispersion of the dispersed phase and its interfacial interaction with the matrix or continuous phase is the initial mechanism for tensile failure in the composite's structure (Adriana et al., 2013; Gamstedt et al., 2011; Khakalo et al., 2018). Herein, we demonstrate that IL-welding can be utilized to enhance the molecular-level dispersion of CNF in PLA.

3.6. Degradation

The degradation of the composite films in seawater was assessed under controlled conditions (25 °C, fixed humidity, and illumination time). Compared to the C/P and pure PLA samples, The D/G-C/P 1 h film showed the highest degradation rate (≈70%, after 7 weeks) (Fig. 4a). The film degradation profile showed a slow initial rate (0.11 wt% per day) followed by an increased degradation rate with time (≈0.2 wt% per day). Although it has been reported that films made from PLA latex show a relatively better degradability in aquatic environments compared to commercial polylactic acid (Ingeo™ manufactured by NatureWorks) (Lee et al., 2016; Martin et al., 2014; Pinto et al., 2015), the pure PLA used in this study only degraded by about 15% after 1 month.

The SEM images of Fig. 4c further illustrate the changes in the surface of the D/G-C/P films during the degradation process (monitored for 7 weeks). Before degradation, the original films had a smooth surface and a solid compact interior (Figs. 4c, w1). The surface became increasingly rougher with time of immersion in seawater, suggesting that degradation started from surface erosion (Lucas et al., 2008). After ≈70% degradation, both the surface and the bulk material clearly collapsed, and perforated structures were observed (Fig. 4c, w7).

Three important degradation molecular mechanisms impact the

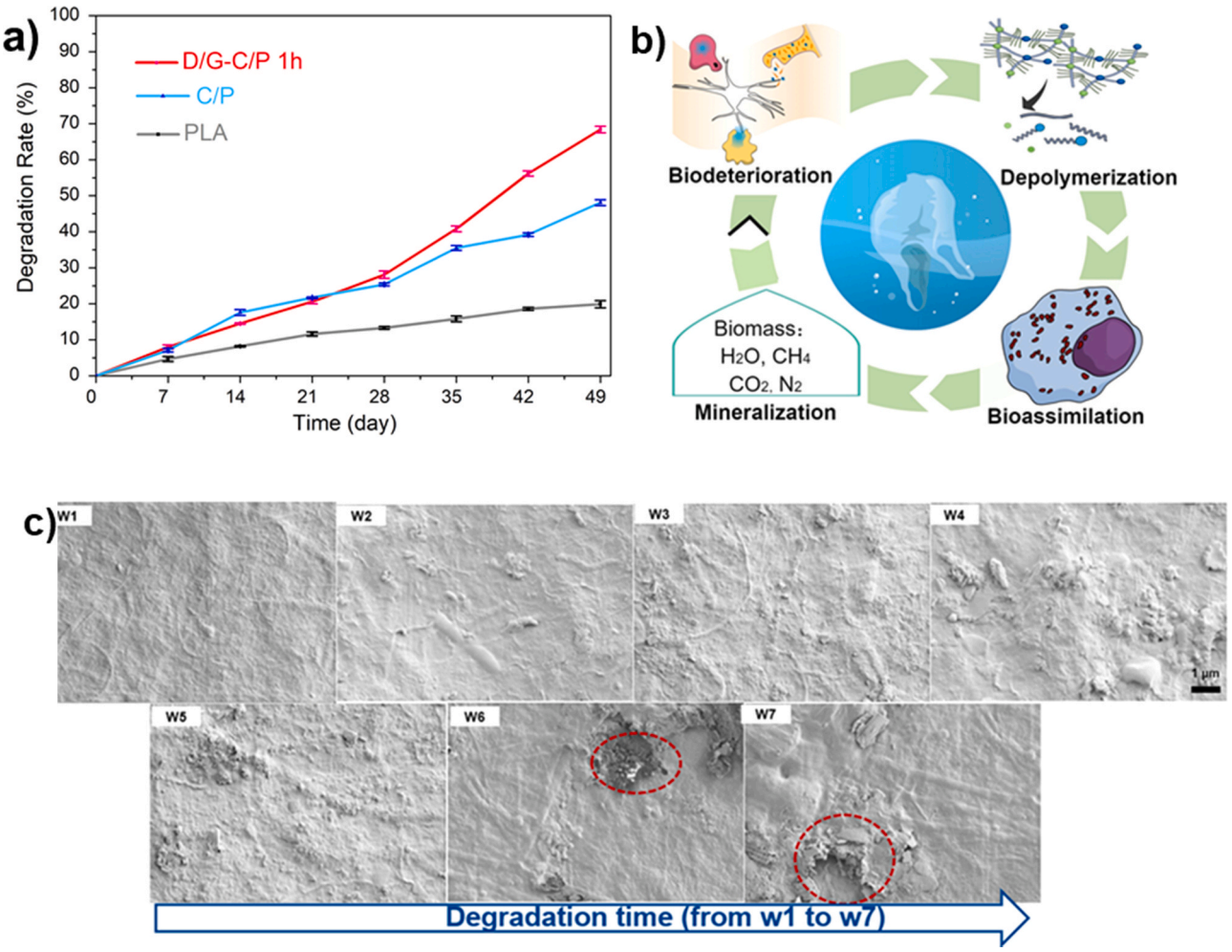

Fig. 4. (a) Degradation rate of C/P, C/P-D/G 1 h, and PLA films in marine water. (b) Schematic illustration of the different steps involved in film biodegradation (from biodeterioration to mineralization). (c) SEM images of the surface morphology of C/P-D/G 1 h film followed from week 1 to week 7 (w1–w7).

physical and thermal properties of plastics in the ocean: surface energy, abiotic hydrolysis, and photodegradation (Ter Halle et al., 2017). The addition of hydrophilic cellulose to PLA improved the hydrophilicity of the composite film, which facilitates the penetration of seawater, leading to fragmentation into smaller pieces (biodeterioration, Fig. 4b). Moreover, the incorporation of "weak links" such as cellulose in the polymer, accelerates abiotic hydrolysis. Compared to densely-bound, semi-crystalline PLA and CNF, the porous and loose structure of IL-welded CNF/PLA films are more susceptible to hydrolysis or degradation. The loosened structure of cellulose subjected to IL treatment, breaking the intra- and intermolecular hydrogen bonds between cellulose chains, is another factor that increases the degradation rate of C/P-D/G. Thus, welded films require less energy for microorganisms and enzymes to catalyze the depolymerization. The proliferation and growth of microorganisms, bacteria, and fungi from the water on the composite films may further accelerate the bioassimiliation of the films and even mineralize them completely (Haider et al., 2019). Although we did not account factors associated with the marine conditions (e.g., salinity, depth in the ocean and mechanical forces), the controlled experiments served as a basis to elucidate the influence of hydrolysis from biodegradation and photoinitiated C–H bond oxidation.

For polymers such as PLA, biodegradation is considered to consist of a sequential mechanism in which the first step is the hydrolysis, which reduces the molecular weight, and is followed by hydrolytic degradation, converting long polymer chains into shorter, water-soluble fragments that become soluble in water (Pantani and Sorrentino, 2013; Zhang et al., 2008). The IL induces changes in the crystallinity of the CNF/PLA composite and introduces a plasticizing effect on PLA. Taken together, it is reasonable to expect that IL welding, not only accelerates the degradation rate of PLA but prevents the polycondensation of shorter PLA into nanoparticles, because of increased water-solubility.

4. Conclusions

Highly stretchable and biodegradable CNF/PLA films were introduced taking advantage of the unique defibrillation ability of IL and the formation of a co-continuous system that involved partially dissolved cellulose, hydrophilic nanofibers and hydrophobic polymers. In particular, IL welding contributed significantly to the biodegradation of PLA/CNF composites in a marine water system by altering the porosity, hydrophobicity, and crystallinity, accelerating biotic and abiotic degradation. Meanwhile, the mechanical properties of the welded films increased dramatically (1 h welding), achieving a tensile strength, strain and Young's modulus of 230 MPa, 13% and 5.4 GPa, respectively. Hence, we offer a facile approach to fabricate a bioplastic (CNF/PLA) that is stronger and more biodegradable than the untreated material.

CRediT authorship contribution statement

Xun Niu: Methodology, Experiments, Software and Characterization, Writing - original draft preparation. **Siqi Huan**: Methodology, Software, Characterization instruction. **Haiming Li**: Software and

Characterization instruction. **Hui Pan**: Supervision, Writing editing. **Orlando J. Rojas**: Supervision, Writing- reviewing and editing.

Declaration of Competing Interest

The authors declare that they have no known competing financial interests or personal relationships that could have appeared to influence the work reported in this paper.

Acknowledgments

Hui Pan and Xun Niu are grateful for the financial support provided by the National Natural Science Foundation of China (No. 31770631). Orlando J. Rojas and Xun Niu acknowledge funding from the Canada Excellence Research Chair initiative, Government of Canada the Canada Foundation for Innovation and the European Research Council under the European Union's Horizon 2020 research and innovation program (ERC Advanced Grant Agreement No. 788489, "BioElCell").

Conflict of interest

The authors declare no conflict of interest.

Appendix A. Supporting information

Supplementary data associated with this article can be found in the online version at doi:10.1016/j.jhazmat.2020.124073.

References

Adriana, G., Jussi, L., Robert, S., Franz, S., 2013. Humidity response of Kraft papers determined by dynamic mechanical analysis. Thermochim. Acta 570, 33–40.
Ahn, S., Chantre, C.O., Gannon, A.R., Lind, J.U., Campbell, P.H., Grevesse, T., O'Connor, B.B., Parker, K.K., 2018. Soy protein/cellulose nanofiber scaffolds mimicking skin extracellular matrix for enhanced wound healing. Adv. Healthc. Mater. 7 (9), 1701175.
Brenckle, M.A., Partlow, B., Tao, H., Applegate, M.B., Reeves, A., Paquette, M., Omenetto, F.G., et al., 2016. Methods and applications of multilayer silk fibroin laminates based on spatially controlled welding in protein films. Adv. Funct. Mater. 26 (1), 44–50.
Clarkson, C.M., El Awad Azrak, S.M., Chowdhury, R., Shuvo, S.N., Snyder, J., Schueneman, G., Ortalan, V., Youngblood, J.P., 2018. Melt spinning of cellulose nanofibril/polylactic acid (CNF/PLA) composite fibers for high stiffness. ACS Appl. Polym. Mater. 1 (2), 160–168.
Deng, Z., Jung, J., Zhao, Y., 2017. Development, characterization, and validation of chitosan adsorbed cellulose nanofiber (CNF) films as water resistant and antibacterial food contact packaging. LWT – Food Sc. Technol. 83, 132–140.
Durkin, D.P., Ye, T., Larson, E.G., Haverhals, L.M., Livi, K.J., De Long, H.C., Shuai, D., et al., 2016. Lignocellulose fiber-and welded fiber-supports for palladium-based catalytic hydrogenation: a natural fiber welding application for water treatment. ACS Sustain. Chem. Eng. 4 (10), 5511–5522.
Fernandes, E.M., Pires, R.A., Mano, J.F., Reis, R.L., 2013. Bionanocomposites from lignocellulosic resources: properties, applications and future trends for their use in the biomedical field. Prog. Polym. Sci. 38 (10–11), 1415–1441.
Gamstedt, E.K., Sandell, R., Berthold, F., Pettersson, T., Nordgren, N., 2011. Characterization of interfacial stress transfer ability of particulate cellulose composite materials. Mech. Mater. 43 (11), 693–704.
Gardella, L., Furfaro, D., Galimberti, M., Monticelli, O., 2015. On the development of a facile approach based on the use of ionic liquids: preparation of PLLA (sc-PLA)/high surface area nano-graphite systems. Green Chem. 17 (7), 4082–4088.
Gordobil, O., Delucis, R., Egüés, I., Labidi, J., 2015. Kraft lignin as filler in PLA to improve ductility and thermal properties. Ind. Crop. Prod. 72, 46–53.
Haider, T.P., Völker, C., Kramm, J., Landfester, K., Wurm, F.R., 2019. Plastics of the future? The impact of biodegradable polymers on the environment and on society. Angew. Chem. Int. Ed. 58 (1), 50–62.
Haverhals, L.M., Foley, M.P., Brown, E.K., Fox, D.M., De Long, H.C., Trulove, P.C., 2012a. Naturalfiber welding: ionic liquid facilitated biopolymer mobilization andreorganization. In: Visser, Ann E. (Ed.), Ionic Liquids: Science and Applications. American Chemical Society,, Washington, DC, pp. 145–166.
Haverhals, L.M., Reichert, W.M., De Long, H.C., Trulove, P.C., 2010. Natural fiber welding. Macromol. Mater. Eng. 295 (5), 425–430.
Haverhals, L.M., Sulpizio, H.M., Fayos, Z.A., Trulove, M.A., Reichert, W.M., Foley, M.P., De Long, H.C., Trulove, P.C., 2012. Process variables that control natural fiber welding: time, temperature, and amount of ionic liquid. Cellulose 19 (1), 13–22.
Jamshidian, M., Tehrany, E.A., Imran, M., Akhtar, M.J., Cleymand, F., Desobry, S., 2012. Structural, mechanical and barrier properties of active PLA–antioxidant films. J. Food Eng. 110 (3), 380–389.
Kaldéus, T., Träger, A., Berglund, L.A., Malmström, E., Lo Re, G., 2019. Molecular engineering of the cellulose-poly (Caprolactone) bio-nanocomposite interface by reactive amphiphilic copolymer nanoparticles. ACS Nano 13 (6), 6409–6420.
Khakalo, A., Filpponen, I., Rojas, O.J., 2018. Protein-mediated interfacial adhesion in composites of cellulose nanofibrils and polylactide: enhanced toughness towards material development. Compos. Sci. Technol. 160, 145–151.
Lee, J.C., Moon, J.H., Jeong, J.H., Kim, M.Y., Kim, B.M., Choi, M.C., Kim, J.R., Ha, C.S., 2016. Biodegradability of poly (lactic acid) (PLA)/lactic acid (LA) blends using anaerobic digester sludge. Macromol. Res. 24 (8), 741–747.
Le Phuong, H.A., Izzati Ayob, N.A., Blanford, C.F., Mohammad Rawi, N.F., Szekely, G., 2019. Nonwoven membrane supports from renewable resources: bamboo fiber reinforced poly (lactic acid) composites. ACS Sustain. Chem. Eng. 7, 11885–11893.
Li, J., Qiu, Z., 2019. Significantly enhanced crystallization of poly (l-lactide) by the synergistic effect of poly (diethylene glycol adipate) and cellulose nanocrystals in their fully biodegradable ternary composite. Ind. Eng. Chem. Res. 58 (34), 15526–15532.
Lin, Y., Patel, R., Cao, J., Tu, W., Zhang, H., Bilotti, E., Bastiaansen, C.W.M., Peijs, T., 2019. Glass-like transparent high strength polyethylene films by tuning drawing temperature. Polymer 171, 180–191.
Lucas, N., Bienaime, C., Belloy, C., Queneudec, M., Silvestre, F., Nava-Saucedo, J.E., 2008. Polymer biodegradation: mechanisms and estimation techniques – a review. Chemosphere 73 (4), 429–442.
Martin, R.T., Camargo, L.P., Miller, S.A., 2014. Marine-degradable polylactic acid. Green Chem. 16 (4), 1768–1773.
Meng, X., Bocharova, V., Tekinalp, H., Cheng, S., Kisliuk, A., Sokolov, A.P., Ozcan, S., et al., 2018. Toughening of nanocelluose/PLA composites via bio-epoxy interaction: mechanistic study. Mater. Des. 139, 188–197.
Min, K., Cuiffi, J.D., Mathers, R.T., 2020. Ranking environmental degradation trends of plastic marine debris based on physical properties and molecular structure. Nat. Commun. 11 (1), 1–11.
Muiruri, J.K., Liu, S., Yeo, J.C.C., Koh, J.J., Kong, J., Thitsartarn, W., Teo, W.S., He, C., 2019. Synergistic toughening of poly (lactic acid)–cellulose nanocrystal composites through cooperative effect of cavitation and crazing deformation mechanisms. ACS Appl. Polym. Mater. 1 (3), 509–518.
Oguz, O., Candau, N., Citak, M.K., Cetin, F.N., Avaz Seven, S., Menceloglu, Y.Z., 2019. A sustainable approach to produce stiff, super-tough, and heat-resistant poly (lactic acid)-based green materials. ACS Sustain. Chem. Eng. 7 (8), 7869–7877.
Olsson, A.M., Salmén, L., Eder, M., Burgert, I., 2007. Mechano-sorptive creep in wood fibres. Wood Sci. Technol. 41 (1), 59–67.
Park, K.I., Xanthos, M., 2009. A study on the degradation of polylactic acid in the presence of phosphonium ionic liquids. Polym. Degrad. Stab. 94 (5), 834–844.
Pantani, R., Sorrentino, A., 2013. Influence of crystallinity on the biodegradation rate of injection-moulded poly (lactic acid) samples in controlled composting conditions. Polym. Degrad. Stab. 98 (5), 1089–1096.
Patterson, A.L., 1939. The Scherrer formula for X-ray particle size determination. Phys. Rev. 56 (10), 978–982.
Pinto, V.C., Ramos, T., Alves, S., Xavier, J., Tavares, P., Moreira, P.M., Guedes, R.M., 2015. Comparative failure analysis of PLA, PLA/GNP and PLA/CNT-COOH biodegradable nanocomposites thin films. Procedia Eng. 114, 635–642.
Raquez, J.M., Habibi, Y., Murariu, M., Dubois, P., 2013. Polylactide (PLA)-based nanocomposites. Prog. Polym. Sci. 38 (10–11), 1504–1542.
Reyes, G., Borghei, M., King, A.W., Lahti, J., Rojas, O.J., 2018. Solvent welding and imprinting cellulose nanofiber films using ionic liquids. Biomacromolecules 20 (1), 502–514.
Rhim, J.W., Park, H.M., Ha, C.S., 2013. Bio-nanocomposites for food packaging applications. Prog. Polym. Sci. 38 (10–11), 1629–1652.
Rodionova, G., Eriksen, Ø., Gregersen, Ø., 2012. TEMPO-oxidized cellulose nanofiber films: effect of surface morphology on water resistance. Cellulose 19 (4), 1115–1123.
Rol, F., Belgacem, M.N., Gandini, A., Bras, J., 2019. Recent advances in surface-modified cellulose nanofibrils. Prog. Polym. Sci. 88, 241–264.
Sharif, A., Mondal, S., Hoque, M.E., 2019. Polylactic acid (PLA)-based nanocomposites: processing and properties. In: Sanyang, M.L., Jawaid, M. (Eds.), Bio-based Polymers and Nanocomposites. Springer, Cham, pp. 233–254.
Soman, S., Chacko, A.S., Prasad, V.S., 2017. Semi-interpenetrating network composites of poly (lactic acid) with cis-9-octadecenylamine modified cellulose-nanofibers from Areca catechu husk. Compos. Sci. Technol. 141, 65–73.
Spence, K.L., Venditti, R.A., Rojas, O.J., Habibi, Y., Pawlak, J.J., 2010. The effect of chemical composition on microfibrillar cellulose films from wood pulps: water interactions and physical properties for packaging applications. Cellulose 17 (4), 835–848.
Ter Halle, A., Ladirat, L., Martignac, M., Mingotaud, A.F., Boyron, O., Perez, E., 2017. To what extent are microplastics from the open ocean weathered? Environ. Pollut. 227, 167–174.
Tripathi, A., Ago, M., Khan, S.A., Rojas, O.J., 2018. Heterogeneous acetylation of plant fibers into micro-and nanocelluloses for the synthesis of highly stretchable, tough, and water-resistant co-continuous filaments via wet-spinning. ACS Appl. Mater. Interfaces 10 (51), 44776–44786.
Urbanek, A.K., Rymowicz, W., Mirończuk, A.M., 2018. Degradation of plastics and plastic-degrading bacteria in cold marine habitats. Appl. Microbiol. Biotechnol. 102 (18), 7669–7678.
Wang, H., Gurau, G., Rogers, R.D., 2012. Ionic liquid processing of cellulose. Chem. Soc. Rev. 41 (4), 1519–1537.
Wang, S., Lu, A., Zhang, L., 2016. Recent advances in regenerated cellulose materials. Prog. Polym. Sci. 53, 169–206.
Wu, B., Zeng, Q., Niu, D., Yang, W., Dong, W., Chen, M., Ma, P., 2019. Design of super toughened and heat-resistant PLLA/elastomer blends by controlling the distribution

of stereocomplex crystallites and the morphology. Macromolecules 52 (3), 1092–1103.
Xu, A., Wang, Y., Gao, J., Wang, J., 2019. Facile fabrication of a homogeneous cellulose/polylactic acid composite film with improved biocompatibility, biodegradability and mechanical properties. Green Chem. 21 (16), 4449–4456.
Yang, Q., Saito, T., Berglund, L.A., Isogai, A., 2015. Cellulose nanofibrils improve the properties of all-cellulose composites by the nano-reinforcement mechanism and nanofibril-induced crystallization. Nanoscale 7 (42), 17957–17963.
Ye, D., Lei, X., Li, T., Cheng, Q., Chang, C., Hu, L., Zhang, L., 2019. Ultrahigh tough, super clear, and highly anisotropic nanofiber-structured regenerated cellulose films. ACS Nano 13 (4), 4843–4853.
Yousefi, H., Nishino, T., Faezipour, M., Ebrahimi, G., Shakeri, A., 2011. Direct fabrication of all-cellulose nanocomposite from cellulose microfibers using ionic liquid-based nanowelding. Biomacromolecules 12 (11), 4080–4085.
Yu, H.Y., Zhang, H., Song, M.L., Zhou, Y., Yao, J., Ni, Q.Q., 2017. From cellulose nanospheres, nanorods to nanofibers: various aspect ratio induced nucleation/reinforcing effects on polylactic acid for robust-barrier food packaging. ACS Appl. Mater. Interfaces 9 (50), 43920–43938.
Zhang, J., Wu, J., Yu, J., Zhang, X., He, J., Zhang, J., 2017. Application of ionic liquids for dissolving cellulose and fabricating cellulose-based materials: state of the art and future trends. Mater. Chem. Front. 1 (7), 1273–1290.
Zhang, T., Fang, L., Lin, N., Wang, J., Wang, Y., Wu, T., Song, P., 2019. Highly transparent, healable, and durable anti-fogging coating by combining hydrophilic pectin and tannic acid with poly (ethylene terephthalate). Green Chem. 21 (19), 5405–5413.
Zhang, X., Espiritu, M., Bilyk, A., Kurniawan, L., 2008. Morphological behaviour of poly (lactic acid) during hydrolytic degradation. Polym. Degrad. Stab. 93, 1964–1970.
Zhu, H., Luo, W., Ciesielski, P.N., Fang, Z., Zhu, J.Y., Henriksson, G., Himmel, M.E., Hu, L., 2016. Wood-derived materials for green electronics, biological devices, and energy applications. Chem. Rev. 116 (16), 9305–9374.
Zhu, M., Wang, Y., Zhu, S., Xu, L., Jia, C., Dai, J., Henderson, D., et al., 2017. Anisotropic, transparent films with aligned cellulose nanofibers. Adv. Mater. 29 (21), 1606284.